Desalination and Water Treatment
www.deswater.com

doi:10.5004/dwt.2021.27217

225 (2021) 300–310
June

Removal and recovery of uranium(VI) from aqueous solution by adsorption of surface aldehyde assembled polystyrene microspheres

Jingbo Ni*, Ruyi Liu, Changhao Yan

School of Chemistry and Chemical Engineering, Yangzhou University, Yangzhou, Jiangsu, 225002, China, Tel./Fax: +86-183-6057-9236; email: 2193359791@qq.com (J.B. Ni), Tel. +86-15312134764; email: 1554359501@qq.com (R.Y. Liu), Tel. +86-13852407595; email: yzuyanch@126.com (C.H. Yan)

Received 28 October 2020; Accepted 4 March 2021

ABSTRACT

The surface aldehyde assembled polystyrene microspheres (PS-CHO) were synthesized via the copolymerization of styrene and acrolein and characterized by Fourier-transform infrared spectroscopy and transmission electron microscopy. Some characteristic parameters, such as specific surface area, pore diameter distribution and zeta potential, were also determined. The content of aldehyde groups in the PS-CHO microspheres was inferred through potentiometric titration. Adsorption of uranium(VI) from an aqueous solution was investigated in a series of variable experiments. Effect of pH value, ionic strength, adsorbent dose, contact time and temperature on uranium(VI) adsorption were also discussed. Results showed that the optimum condition was the temperature of 313 K, 0.4 g L^{-1} of adsorbent dosage, pH value of 6.0 for 20 mg L^{-1} of uranium(VI) concentration. The maximum removal efficiency of uranium(VI) ions was 92.13%. Kinetic studies certified the pseudo-second-order was the best-suited model and the fitting linear plot of the intraparticle diffusion model did not pass the origin, indicating that chemical sorption was the rate-determining step of the adsorption mechanism rather than mass transfer. Also, the Elovich equation was consistent with the experimental data, meaning chemical interactions between microspheres and adsorbates. The adsorption capacity at the equilibrium of PS-CHO microspheres was estimated to be 46.07 mg g^{-1} at 313 K. Furthermore, about 96% of adsorbed uranium(VI) could be recovered by laconic perchloric acid treatment, suggesting the stability and reusability of PS-CHO microspheres.

Keywords: Uranium; Polystyrene; Microspheres; Adsorption; Kinetic; Recovery

1. Introduction

Uranium is a strategic resource for military and civilian industries and a toxic radioactive element for the environment [1–3]. Over the past decade, due to the sustainable commercial development in nuclear energy, excessive amounts of uranium have transpired into water systems all over the world [4,5], causing a series of health risks or even death for humans and animals [6]. The World Health Organization (WHO) has determined that the concentration of uranium(VI) in water should not exceed 50 μg L^{-1} [7]. The drinking water standard recommended by U.S. Environmental Protection Agency (EPA) is 20 μg L^{-1} for 238U [8]. Therefore, it is essential to remove the uranium from wastewater for preventing radioactive contamination and recover the uranium for long-term resource availability.

Up to now, several methods such as adsorption [9], photocatalytic purification [10], microwave catalysis [11] and catalytic ozonation [12], have been applied for the decontamination of toxicants from aqueous solution. Photocatalysis has huge advantages since it utilizes solar energy directly for the degradation [13]. Microwave can rapidly and selectively heat the surface active sites of the catalyst and generate strong oxidizing free radicals to degrade the organic

* Corresponding author.

contaminants [14]. Notably, for those two aforementioned techniques, the additional driving force are indispensable in the process. Catalytic ozonation is a promising advanced technology, the excellent performance is ascribed to the reaction between molecular ozone and OH radical. However, the reaction conditions were rather complicated and unsuitable for practical applications. Recently, particular attention has focused on the adsorption of heavy metals from wastewater environment due to the easy operation and inexpensive cost in industries [15]. Meanwhile, the influence of the adsorbents on the adsorption results cannot be ignored either. Therefore, it is a clear direction for the investigation of advanced adsorbents with enhanced adsorption rates and capacities.

Nanomaterials, such as graphitic-like carbon nitride (g-C_3N_4) [16] and covalent organic frameworks [17], have attracted extensive enthusiasm by researchers in the absorption owing to their stable properties, low-cost and environmentally friendly features [18]. Tan et al. [19] fabricated a three-dimensional layered material via *in situ* growth of hydroxide nanosheet arrays onto graphene. This composite has a large surface area and typical mesoporous properties, the maximum sorption capacity for uranium(VI) was 277.80 mg L^{-1} at pH 4.00. Huang et al. [20] synthesized a kind of porous Al_2O_3 by the calcination of MIL-53 (Al). The result showed that the homogeneous and well-dispersed microspheres can effectively remove U(VI)/Eu(III) from real radioactive seawater within an extremely short time. The superior performance in the absorption could be attributed to the high specific surface area, sorption selectivity and abundant functional groups of those nanomaterials, the strong complexes formed with heavy metals on the surface was the adsorption sites for ions. However, the polymer materials modified by surface functional group assembly had a few reports on eliminating pollutants from aqueous solutions [21].

Taking all the aforementioned factors into consideration, the surface aldehyde-assembled polystyrene microspheres (PS-CHO) were first prepared via the copolymerization of styrene and acrolein and applied for the removal and recovery of radioactive wastes from the low concentration aqueous solution. Uranyl acetate dihydrate was chosen as the representative pollutant. Factors affecting the adsorption process such as pH, adsorbent dose, ionic strength, contact time and temperature have been investigated. Adsorption kinetics was calculated using pseudo-first-order, pseudo-second-order, Elovich equation and intraparticle diffusion model. The mechanism of the adsorption process was also discussed.

2. Materials and methods

2.1. Materials and reagents

Uranyl acetate dihydrate ($UO_2(CH_3COO)_2{\cdot}2H_2O$), hydrochloric acid (HCl), nitric acid (HNO_3), perchloric acid ($HClO_4$) were purchased from Sinopharm Chemical Reagent Corporation (China) and used as received. Polyvinylpyrrolidone (PVP, K13-18), azobisisobutyronitrile (AIBN), styrene (ST), acrolein (C_3H_4O), glacial acetic acid (CH_3COOH), sodium chloride (NaCl), sodium nitrate ($NaNO_3$), calcium nitrate ($Ca(NO_3)_2$) were purchased from Shanghai Aladdin Bio-Chem Corporation (China) and are of A.R. grade. The ultrapure water was prepared in our laboratory.

2.2. Sample preparation

Initially, 2.5 g of PVP was thoroughly dissolved in 40 mL of ethanol (solution A). Then, 0.15 g of AIBN was dissolved in 9 mL of styrene (solution B). Next, the two solutions above were mixed with stirring and heating at 70°C for 30 min. After the solution became milky white, 6 mL of acrolein was added thereto and kept the sustained reaction for 8 h. After the reaction system was cooled to room temperature, the obtained white suspension was collected by centrifuging at 10,000 rpm for 15 min and washed three times with ethanol. The product was dried in a vacuum at 40°C for 24 h.

2.3. Characterization

The morphology of PS-CHO microspheres was performed by transmission electron microscopy (TEM, JEM-2100, Japan). The functional groups of PS-CHO microspheres were analyzed using Fourier-transform infrared spectroscopy (FTIR, Antains II, America), the samples were compressed with dried potassium bromide (KBr) powder. The chemical states were characterized by X-ray photoelectron spectroscopy (XPS, ESCALAB 250Xi, America). Thermogravimetric analysis (TGA, Pyris, America) was conducted at a heating rate of 10°C/min in nitrogen from room temperature to 800°C. The specific surface area of PS-CHO microspheres was calculated by Brunauer–Emmett–Teller (BET) method. The pore diameter distribution was determined by the Barrett–Joyner–Halenda (BJH) model using the desorption branch of the isotherm [22]. The zeta potential analyzer (Zetasizer ZS90, Austria) was measured at pH values from 2.1 to 10.2 [23].

2.4. Adsorption experiments

The uranium(VI) solution was prepared by $UO_2(CH_3COO)_2{\cdot}2H_2O$ and deionized water. Initially, 40 mg PS-CHO microspheres were added into the uranium(VI) solution (100 mL, 20 mg L^{-1}) in a three-necked flask under the stirring of 315 r/min. At specific intervals, the suspension was taken out via an injector equipped with membrane filters (d = 0.23 μm) and separated. The residual concentration of uranium(VI) in the liquid phase was monitored by UV-Vis adsorption spectrometer (UV-2550, Shimadzu, Japan) at the absorbance λ_{max} = 651 nm [24]. The adsorption capacities of uranium(VI) by PS-CHO microspheres in aqueous solution were calculated as the following equation:

$$q_e = \frac{V\left(C_0 - C_e\right)}{m} \tag{1}$$

2.5. Desorption studies

Desorption tests were conducted after the adsorption equilibrium, the experiments were implemented with dried PS-CHO microspheres (0.2 g) loaded with known amounts of uranium(VI). Five different kinds of desorption solutions (ultrapure water, 0.1 mol L^{-1} NaCl, 0.1 mol L^{-1} HCl, 0.1 mol L^{-1}

HNO_3 and 0.1 mol L^{-1} $HClO_4$) were selected as desorption medium. Each experiment was performed for 2 h at room temperature. Subsequent experiments were also carried out to test the stability and reusability of adsorbents. After each cycle, the PS-CHO microspheres were separated by centrifuging at 8,000 rpm for 10 min and washed three times with ethanol.

3. Results and discussion

3.1. Characterization of adsorbent

The TEM images of the PS-CHO microspheres before and after contacting with uranium(VI) are shown in Fig. 1a and b, respectively. The morphology of PS-CHO microspheres was perfect spheres and exhibited well-defined spherical outlines and smooth surfaces with a diameter of 210 nm. Additionally, some amount of nanosheet-like precipitation were gathered on the surface of PS-CHO microspheres after contacting with uranium(VI). The energy-dispersive X-ray spectroscopy (EDS) spectrum of the PS-CHO microspheres after contacting with uranium(VI) exhibited distinct peaks of C, O, Cu and U (Fig. 1c), indicating the presence of these elements. high angle annular dark field-scanning transmission electron microscopy (HAADF-STEM) images further proved that the uranium oxide (U_xO_y) nanoparticles were formed on the microspheres (Fig. 1d).

In order to verify the aldehyde groups on the surface of microspheres, the FTIR spectrum was measured (Fig. 2a). Four peaks in the range of 3,082–3,001 cm^{-1} were ascribed to the sp^2 C–H stretching vibrations of phenol [25]. The characteristic peaks at around 1,493 and 1,452 cm^{-1} were caused by the sp^2 C–H bending vibration of –C=C–. Three distinctive peaks at 1,069; 1,028 and 756 cm^{-1} represented the C–H deformation vibration of single-substituted phenol. Moreover, the presence of C=O absorption peak at 1,710 cm^{-1} and the C–H absorption peak of the aldehyde group at 2,720 cm^{-1} demonstrated that a polymerization reaction has occurred and the aldehyde groups were anchored on the surface of microspheres [26].

N_2 adsorption/desorption isotherm and pore diameter distribution of the PS-CHO microspheres were examined for

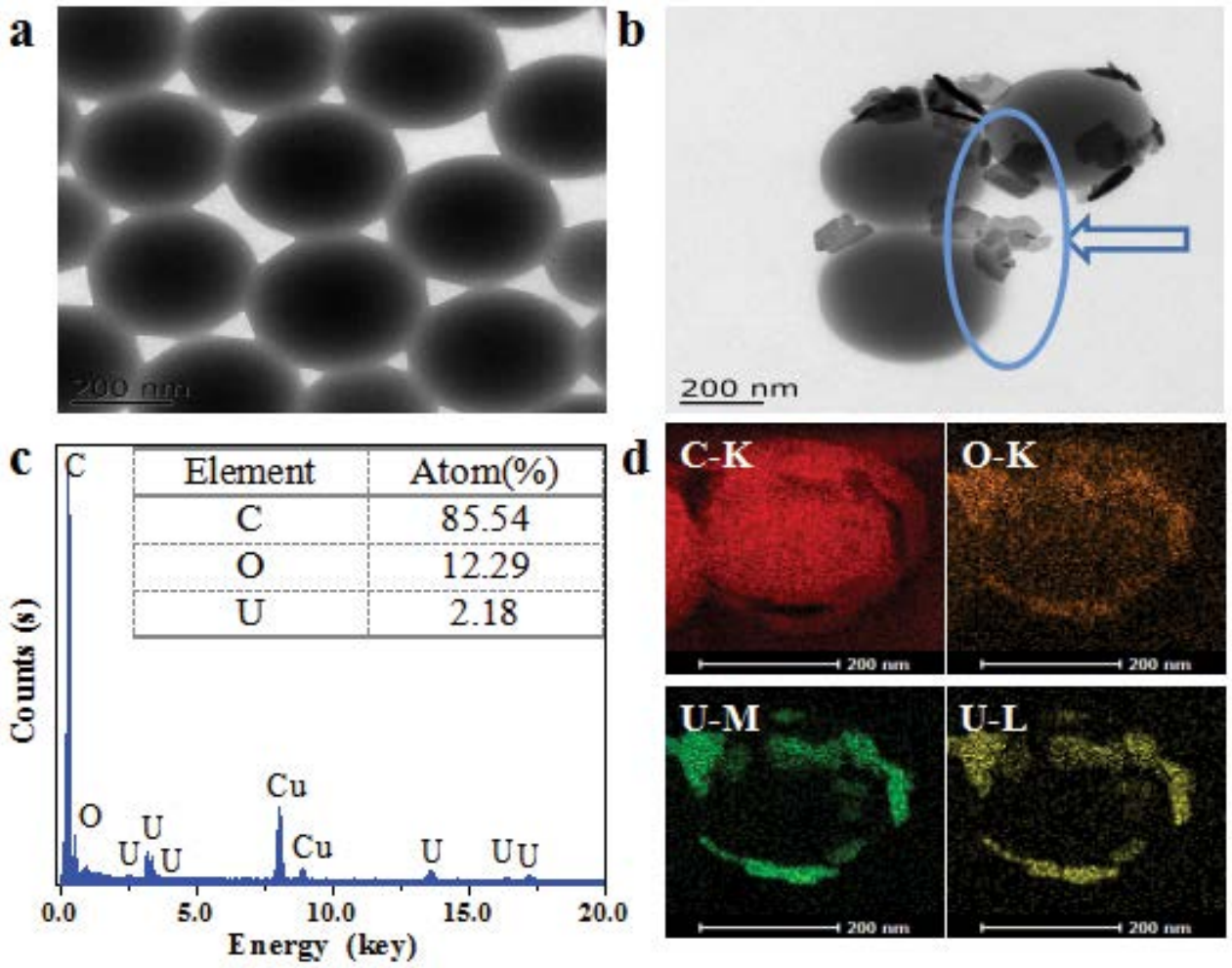

Fig. 1. (a) TEM image of PS-CHO microspheres before reaction with uranium(VI), (b) TEM image of PS-CHO microspheres after reaction with uranium(VI), (c) EDS spectrum of uranium(VI)-loaded PS-CHO microspheres, (d) HAADF-STEM images of uranium(VI)-loaded PS-CHO microspheres.

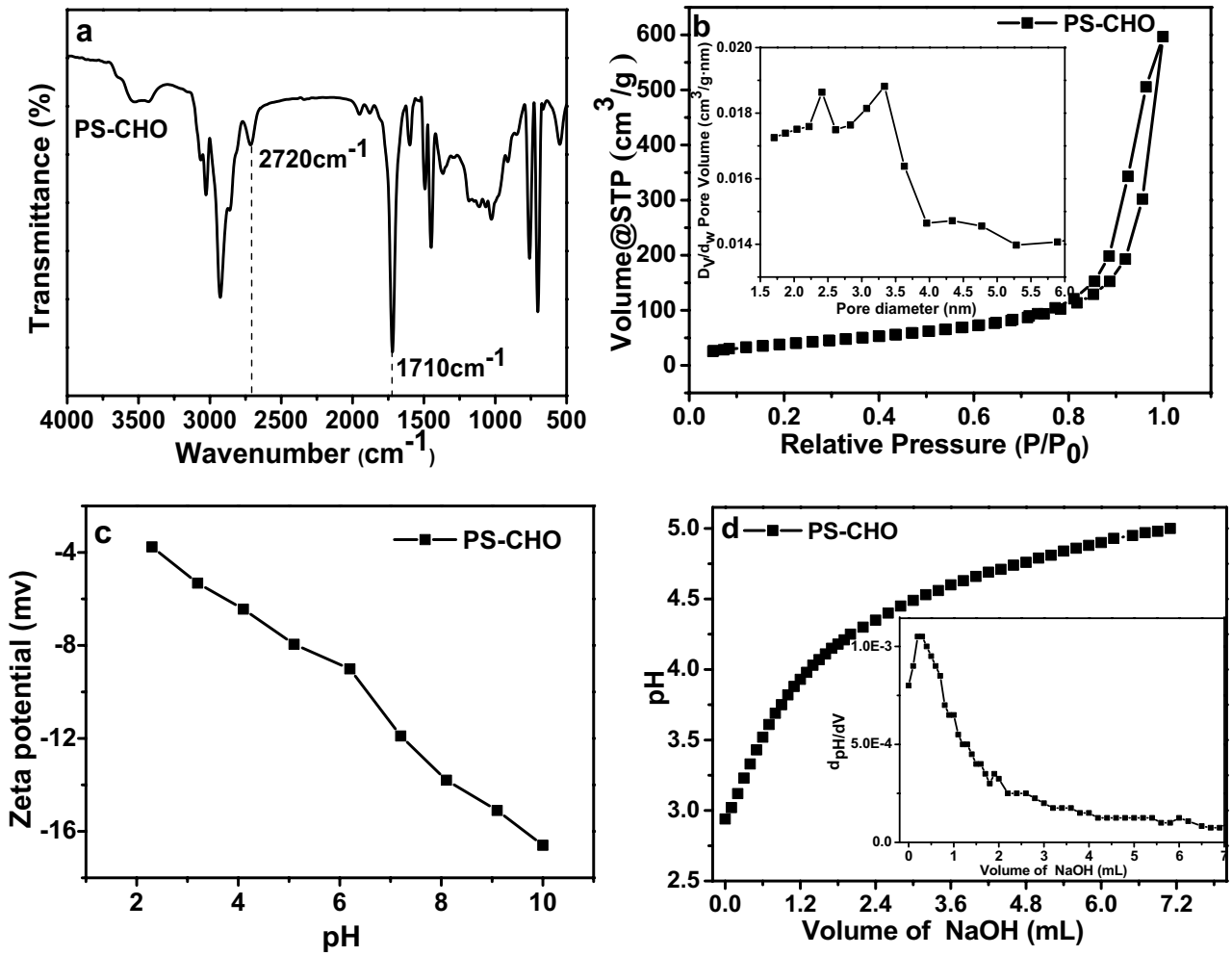

Fig. 2. FTIR spectrum (a), N_2 adsorption–desorption isotherm and pore diameter distribution (inset) (b) and zeta potentials (c) of PS-CHO microspheres, (d) potentiometric titration curve of PS-CHO microspheres and first-order differential curve (inset).

the investigation of structure [27]. As displayed in Fig. 2b, no secondary uptake appeared at a low relative pressure ($P/P_0 < 0.4$), suggesting the adsorption isotherm could be classified as type IV [28]. However, H_3-type hysteretic loop was appeared at high pressure ($P/P_0 > 0.7$), implying the atactic pore structure of microspheres [29]. More detailed explanation was revealed by BET analysis. The specific surface areas of PS-CHO microspheres calculated by the BET equation was 145.92 $m^2\ g^{-1}$. Furthermore, the pore diameter distribution of microspheres determined by the BJH model was centered at 2.04–3.33 nm. Based on the reported researches, a high specific surface area made PS-CHO microspheres one of the efficient adsorbents. The zeta potentials of PS-CHO microspheres are recorded in Fig. 2c, higher the pH value, lower the potentials and more negative charges, suggesting that electrostatic attraction may be one of the adsorption mechanisms [30]. The content of aldehyde groups in the PS-CHO microspheres was determined through potentiometric titration and carried out with 50 mg of PS-CHO microspheres against sodium hydroxide (0.01 mol L^{-1}) solution [31]. The titration was continued till the completion of de-protonation. Drew the pH-V_{NaoH} titration plot in OriginPro8 (Fig. 3d) and differentiated once [32]. The content of aldehyde groups was consistent with the peak point of the differential curve (Fig. 2d inset) and was found to be 0.03 mol g^{-1} which matches with the contemplated value. The calculation equations are as follows:

$$\mathrm{PS-(CHO)}_n + n\mathrm{H_2N-OH-HCl} = \mathrm{PS-(CH=N-OH)}_n + n\mathrm{H_2O} \quad (2)$$

$$\mathrm{HCl + NaOH = NaCl + }n\mathrm{H_2O} \quad (3)$$

$$\Delta V \times 0.01 \times n_{\mathrm{NaCl}} = n_{\mathrm{CHO}} \quad (4)$$

$$[\mathrm{CHO}] = \frac{n_{\mathrm{CHO}}}{W_{\mathrm{PS-CHO}}} \quad (5)$$

The chemical states of PS-CHO microspheres after contacting with uranium(VI) were further investigated by XPS measurement to demonstrate the surface elemental composition. As shown in Fig. 3a, the U4f bond energy

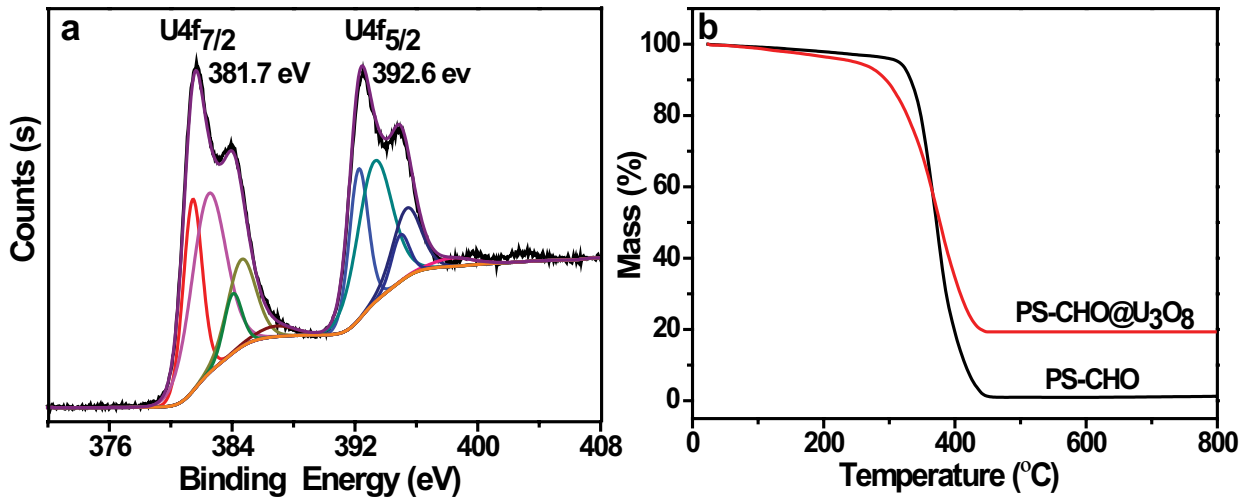

Fig. 3. (a) XPS survey spectrum of PS-CHO@U_3O_8:U4f and (b) TGA curves of PS-CHO microspheres and PS-CHO@U_3O_8 microspheres.

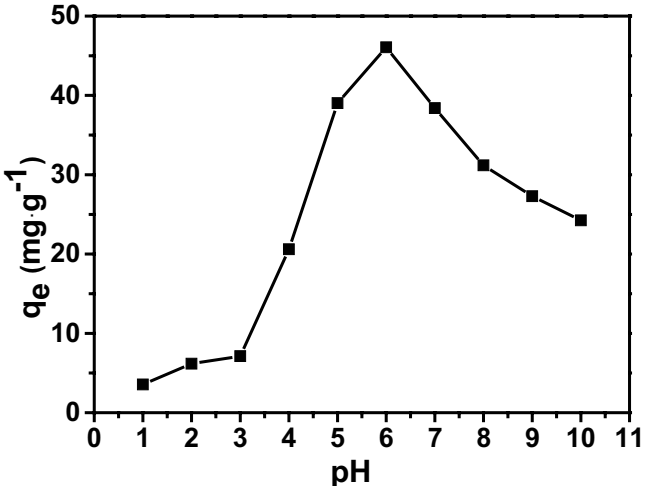

Fig. 4. Effect of pH value on uranium(VI) adsorption in aqueous solution.

peak at 381.7 and 392.6 eV were corresponding to the $U4f_{7/2}$ and the $U4f_{5/2}$, respectively. This result was consistent with the reported articles by the study of Zhang et al. [33]. Meanwhile, the satellite peaks were emerged at higher binding energy after Lorentz–Gaussian fitting, suggesting the U4f spectrum was formed by the superposition of the UO_2 spectrum and UO_3 spectrum [34,35]. The peak areas ratio of U(IV) and U(VI) after calculation was 1:1.26, demonstrating the precipitates on the surface of PS-CHO microspheres after reaction were triuranium octoxide (U_3O_8). The content of U_3O_8 was quantitatively analyzed by TGA (Fig. 3b). For the PS-CHO microspheres, there was almost no weight loss at temperatures above 450°C, indicating the thorough combustion process. For the PS-CHO@U_3O_8 composite microspheres, 19.07% of the weight remained at 450°C and then the curve became constant, concluding that the content of U_3O_8 was 19.07 wt.%.

3.2. Adsorption performance

3.2.1. Effect of pH value

The pH of aqueous solution is a key factor for adsorption performance. Adsorption of uranium(VI) on PS-CHO microspheres was studied by adjusting the pH of initial solution between 2 and 10 with 0.1 mol L^{-1} HCl or 0.05 mol L^{-1} NaOH. As shown in Fig. 4, at pH < 3, the predominant uranium(VI) are uranyl ions (UO_2^{2+}) [36], since the limited complexing sites caused by the competition of hydrogen ions (H^+) and UO_2^{2+} ions, the adsorption was observed to be less. At weakly acidic condition (pH 5–6), the UO_2^{2+} ions were hydrolyzed and formed $UO_2(OH)^+$, $(UO_2)_2(OH)_2^{2+}$ and $(UO_2)_3(OH)^{5+}$ ions with positive charges [37], the adsorption rate of uranium(VI) raised rapidly due to the formation of electrostatic adhesion, the maximum adsorption efficiency of PS-CHO microspheres was obtained at pH 6. In strong alkaline solution, the UO_2^{2+} ions were presented in the anionic form by integrating with hydroxyl anions [38], which has less interaction with aldehyde groups of microspheres. Therefore, all succeeding experiments were carried out at pH 6.0.

3.2.2. Effect of PS-CHO microspheres dosage

The influence of PS-CHO microspheres dosage on the adsorption process is shown in Fig. 5. Experimental results revealed that adsorption efficiency of uranium(VI) increased with increasing adsorbent dosage, which attributed to the increase of the active binding sites. 93.12% of uranium was removed from 100 mL solution containing 20 mg L^{-1} uranium(VI). Correspondingly, the adsorption capacities gradually decreased with increasing adsorbent dosage. This could be summarized in the decrease of adsorption driving force and the excess of aldehyde groups which could not be effectively used.

3.2.3. Effect of contact time and temperature

Fig. 6 illustrates the contact time and temperature profiles of uranium(VI) adsorption on PS-CHO microspheres

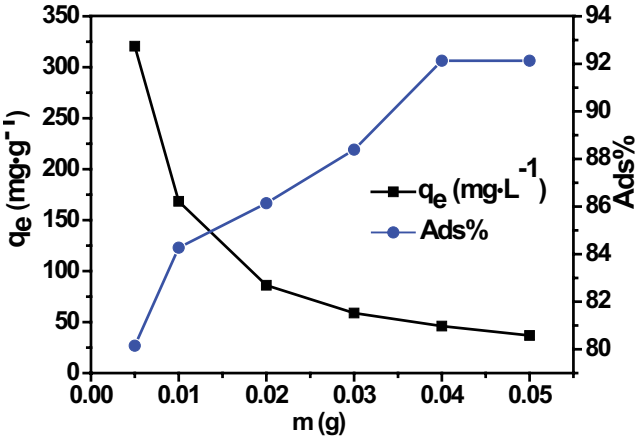

Fig. 5. Effect of PS-CHO microspheres dosage on uranium(VI) removal.

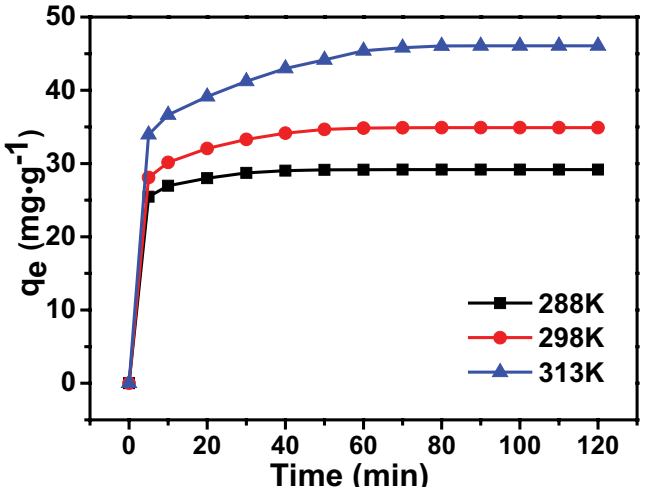

Fig. 6. Effect of contact time and temperature on uranium(VI) adsorption in aqueous solution.

in terms of adsorption capacities. It was observed that the adsorption was rapidly in 5 min and then attained equilibrium gradually within 90 min, suggesting the strong chemical surface interactions between uranium(VI) ions and PS-CHO microspheres. The rapid adsorption rate demonstrated the high efficiency of adsorbents and certified that 90 min is enough to achieve equilibrium. Meanwhile, the results also revealed that the adsorption capacities increased significantly at the higher temperature, indicating that heating is beneficial to promote the adsorption process. The adsorption capacity at equilibrium was 46.07 mg g^{-1} at the temperature of 313 K in 90 min, therefore, the PS-CHO microspheres in this study presented appropriate adsorption capacity in comparison with other adsorbents [39–43].

3.2.4. Effect of ionic strength

Considering various electrolytes reserved in real radioactive wastewater, sodium chloride (NaCl), sodium

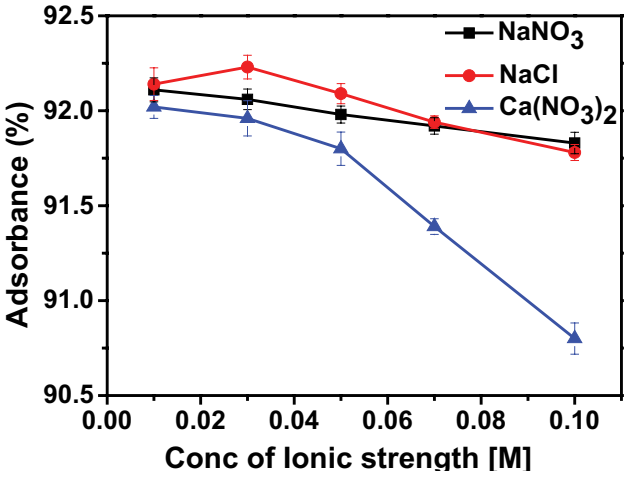

Fig. 7. Effect of ionic strength on uranium(VI) adsorption in aqueous solution.

nitrate ($NaNO_3$) and calcium nitrate ($Ca(NO_3)_2$) were used to simulate different adsorption environment. The influence of ionic strength in the concentration range of 0.01 to 0.1 mg L^{-1} on uranium(VI) adsorption was discussed. Fig. 7 shows the concentration of $NaNO_3$ has no significant effect on adsorption. However, in the presence of NaCl, the adsorption percentage of U(VI) adsorption increased with increasing concentration and then decreased. The initial increase may be attributed to the formation of [UO_2(OH)Cl] which enhanced the adsorption process [44]. The anionic chloro complex of uranium(VI) formed at high NaCl concentration may resulted in the reduced adsorption [45]. Also, a gradual decrease of adsorption was observed in presence of $Ca(NO_3)_2$, the addition of metal cations (Ca^{2+}) increased the competition between the target ions and the binding sites of PS-CHO microspheres.

3.3. Adsorption kinetic

Four different kinetic models were employed for investigating the mechanism of uranium(VI) adsorption on PS-CHO microspheres. Pseudo-first-order (Eq. (6)) and pseudo-second-order (Eq. (7)) are commonly used for describing the physisorption behavior and chemisorption process between target pollutants and adsorbents, respectively [46]. Elovich equation (Eq. (8)) is related to the energy of chemical adsorption varying with the surface coverage [47]. Intraparticle diffusion model (Eq. (9)) is used to estimate a diffusion controlled reaction rate. The goodness of consistency between experimental data and the kinetic models values is expressed by the relative coefficient (r^2). Several high r^2 value indicate that the model successfully described the adsorption kinetics. The linear mathematical expressions of these models are as follows:

$$\ln(q_{e,1} - q_t) = \ln q_{e,1} - k_1 t \tag{6}$$

$$\frac{t}{q_t} = \frac{1}{k_2 q_{e,2}^2} + \frac{t}{q_{e,2}} \tag{7}$$

$$q_t = a + b\ln(t) \quad (8)$$

$$q_t = k_3 t^{0.5} + s \quad (9)$$

Form the linear plots of $\ln(q_e - q_t)$ vs. t (Fig. 8a) and t/q_t vs. t (Fig. 8b), the related parameters were summarized in Tables 2 and 3. Apparently, the relative coefficient (r^2) of the pseudo-second-order model were all >0.999 compared with those of pseudo-first-order model ($r^2 < 0.969$), revealing the better description than of pseudo-first-order model. Moreover, the q_e values by experiments were in agreement with the ones obtained from the fitting of pseudo-second-order model, evidencing that chemical sorption between the uranium(VI) ions and the binding sites might be rate-determining step of adsorption mechanism in solution consequently [48], which arose from valence forces through sharing or exchanging electrons between absorbent and absorbate [49].

Elovich equation was used to further investigate the potential adsorption mechanism. As illustrated in Fig. 8c and Table 4, a high relatively correlation coefficient (r^2 = 0.9889) suggested that the Elovich equation fitted the experiment points very well, indicating the chemical interactions between the adsorption sites on PS-CHO microspheres surface and uranium(VI) in aqueous solution [50].

The mass transfer of uranium(VI) from bulk solution to the surface of PS-CHO microspheres is related to physical or chemical adsorption [51]. The intraparticle diffusion model and the regression parameters are presented in Fig. 8d and Table 5, respectively. If the diffusion plot of q_t vs. $t^{0.5}$ is a straight line and the intercept is zero, the intraparticle diffusion model was the rate-controlling step [52]. However, Fig. 8d clearly shows that the adsorption process followed two stages: a quick sorption process and equilibrium stage. In addition, the fitting linear plot did not pass through the origin, meaning that the intraparticle diffusion rate is not only controlling step of the adsorption process. Values of intercept (s) represented the thickness of boundary layer. The order of intercept was $s_{288K} < s_{298K} < s_{313K}$, suggesting the increasing boundary layer effect [53].

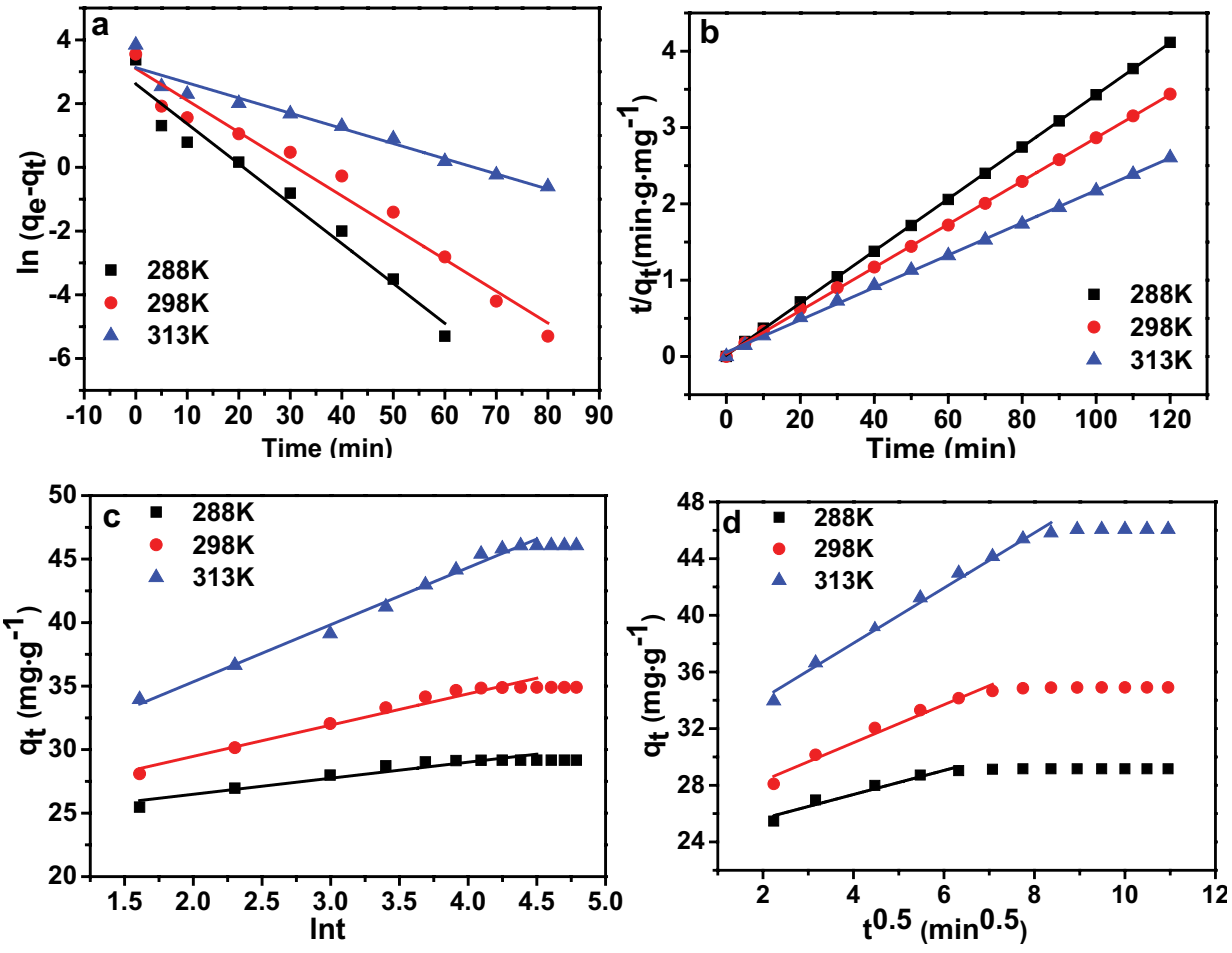

Fig. 8. Kinetic studies for uranium(VI) adsorption according to pseudo-first-order model (a and b) pseudo-second-order model, (c) Elovich model, and (d) intraparticle diffusion model.

Table 1
Comparison of adsorption capacity for uranium(VI) with various adsorbents

Adsorbent	q_e (mg g^{-1})	Adsorption conditions				References
		Contact time (min)	Dosage (g L^{-1})	pH	T (K)	
PS-CHO microspheres	46.06	60	0.4	6.0	313	This study
Polyacrylonitrile fibers	15.92	480	1.0	5.0	298	[39]
Activated carbon fibers	35.47	60	1.0	6.0	318	[40]
Ca–Mg–Al layered double hydroxide	65.36	120	0.1	5.0	298	[41]
Magnetic biochar	54.4	720	1.0	3.0	293	[41]
Mesoporous carbon	73.75	40	1.2	3.0	333	[42]
Rutile TiO_2	1.9	5	1.0	4.0	298	[42]
Fe_3O_4@SiO_2	0.0441	120	2.0	5.0	298	[43]

Table 2
Kinetic parameters for uranium(VI) adsorption on PS-CHO microspheres in pseudo-first-order equation

Parameter	k_1 (min^{-1})	$q_{e,1}$ (mg g^{-1})	r^2	SD
Temperature (K)				
288	0.1252	13.6810	0.9610	0.3211
298	0.0998	22.1935	0.9692	0.2678
313	0.0476	22.8648	0.9452	0.1724

Table 3
Kinetic parameters for uranium(VI) adsorption on PS-CHO microspheres in pseudo-second-order equation

Parameter	k_2 (g mg^{-1} min^{-1})	$q_{e,2}$ (mg g^{-1})	r^2	SD
Temperature (K)				
288	0.0622	29.4118	0.9996	0.0041
298	0.0233	35.3357	0.9998	0.0069
313	0.0086	47.1698	0.9991	0.0115

Table 4
Kinetic parameters for uranium(VI) adsorption on PS-CHO microspheres in Elovich equation

Parameter	a (mg g^{-1})	B (g mg^{-1} min^{-1})	r^2	SD
Temperature (K)				
288	23.7586	1.3374	0.9278	0.4616
298	24.5477	2.4609	0.9647	0.5681
313	26.3469	4.6959	0.9889	0.5741

Table 5
Kinetic parameters for uranium(VI) adsorption on PS-CHO microspheres in intraparticle diffusion model

Parameter	k_3 (mg g^{-1} min$^{-0.5}$)	s (mg g^{-1})	r^2	SD
Temperature (K)				
288	0.8491	23.9545	0.9349	0.5090
298	1.3416	25.6396	0.9668	0.5635
313	2.0389	29.8705	0.9939	0.3601

3.4. Desorption and reusability study

Recovery and reusability are important elements for adsorbents, the outstanding performance in recycling significantly reduced the capitalized development cost in industrial applications. The desorption efficiencies of uranium(VI) are illustrated in Fig. 9a to prove the reusability capacity of PS-CHO microspheres, it was found that the desorption increased obviously at the time scope of 0–10 min, and then began to slow down till the desorption equilibrium. The influence of desorption solutions was also discussed (Fig. 9b). The ultrapure water and sodium chloride (0.1 mol L^{-1} NaCl) showed negligible desorption effect for PS-CHO microspheres loaded with U_3O_8 (less than 2%). However, the inorganic acids (0.1 mol L^{-1} HCl, 0.1 mol L^{-1} HNO_3 and 0.1 mol L^{-1} $HClO_4$) resulted in high desorption efficiencies of uranium(VI) about 80.16%, 86.77% and 95.63%, respectively. This result proved that the perchloric acid is the optimum desorption solution. After desorption equilibrium, the reusability of recycled PS-CHO microspheres was tested. The adsorption capacities were sustainably decreased with the increasing of cycle times (Fig. 9c). This interesting result may associate with limited binding sites. Additional, the dispersion of microspheres decreased due to the irregular deformation causing by perchloric acid. Meanwhile, the residual U_3O_8 nanoparticles still occupied the binding sites, which has less adsorption capacity since the stereo-hindrance effect, thus the deposition of fresh uranium(VI) on the surface of PS-CHO microspheres was prevented.

3.5. Adsorption mechanism

According to the aforementioned researches, the dominate adsorption mechanism was the electrostatic attraction between the adsorbent and adsorbate. As illustrated in Fig. 10, when uranium(VI) ions crossed the diffusion layer and then entered into adsorption layer in aqueous solution, the aldehyde groups of PS-CHO microspheres could captured the target and formed the surface complexes. Oxygen reserved in the reaction system was the oxidant, and then triuranium octoxide (U_3O_8) nanoparticles were precipitated on the PS-CHO microspheres.

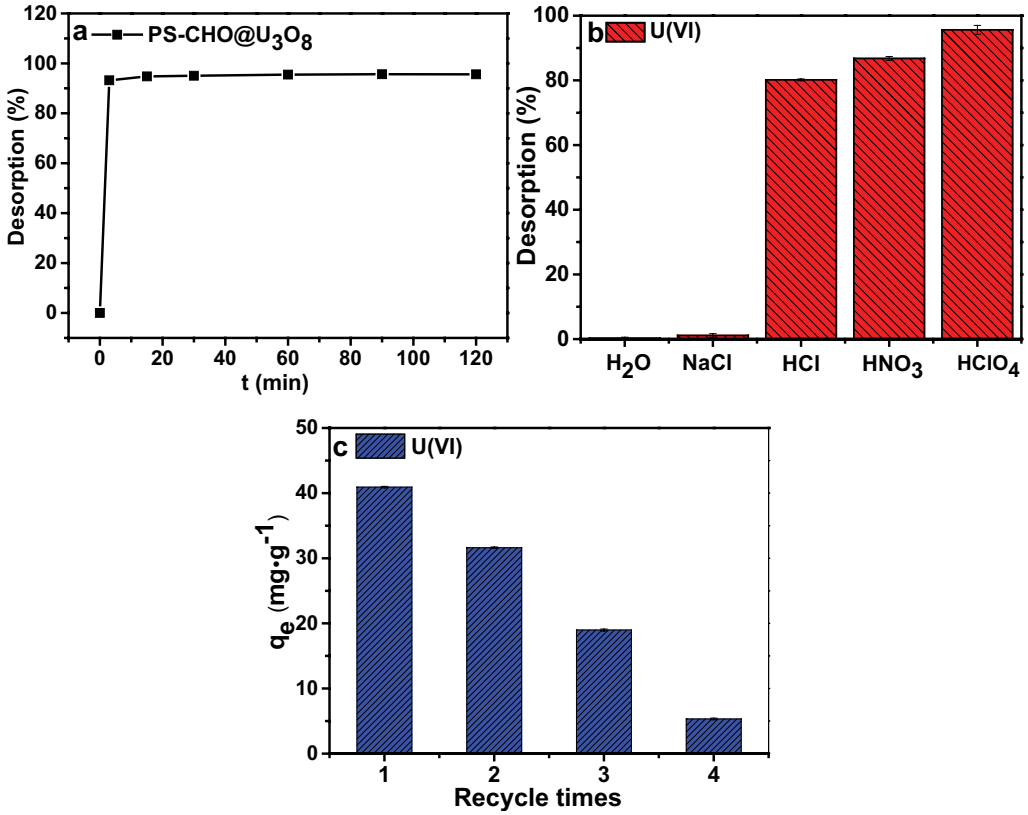

Fig. 9. Desorption efficiencies of uranium(VI) (a) within 120 min in 0.1 mol L^{-1} $HClO_4$, (b) the influence of different desorption solution on uranium(VI) adsorption, and (c) the adsorption capacities of PS-CHO microspheres with different recycle times.

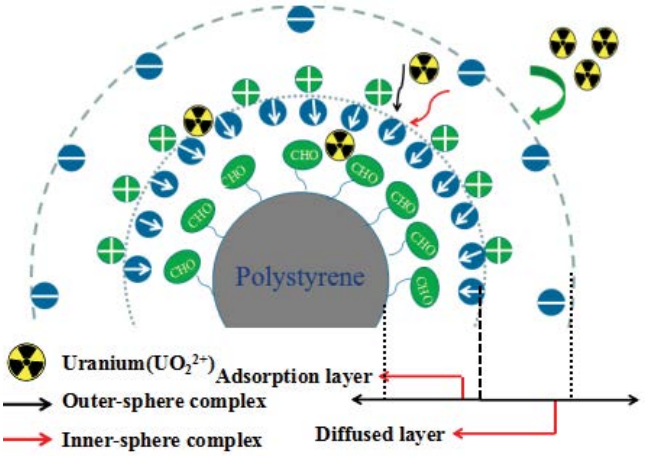

Fig. 10. Schematic illustration of the uranium(VI) adsorption of PS-CHO microspheres.

4. Conclusions

In this study, the surface aldehyde assembled polystyrene microspheres (PS-CHO) were fabricated, characterized and applied in removal and recovery of uranium(VI) from aqueous solution. The prepared samples with perfect spherical outline and well-dispersed microspheres effectively removed uranium(VI) ions from aqueous solution within extremely short time. The adsorption capacity was observed to be dependent on pH value, ionic strength, adsorbent dose and contact time and temperature. The adsorption efficiency at equilibrium of PS-CHO microspheres was estimated to be 46.07 mg g^{-1} at pH 6.0 and the optimum condition for was temperature of 343 K, 0.4 g L^{-1} of adsorbent dosage for 20 mg L^{-1} of uranium(VI) concentration. Kinetic dates fitted pseudo-second-order very well and intraparticle diffusion model did not passed the origin, indicating the chemical adsorption is the rate-controlling step. Elovich equation further proved chemical interactions between microspheres and adsorbates. The perchloric acid ($HClO_4$) was the best desorption solution for recovery of uranium(VI). These results demonstrated the PS-CHO microspheres are excellent adsorbent for the elimination of uranium.

Symbols

C_0 — Initial concentration of metal ion in solution, mg L^{-1}

C_e — Concentration of metal ion in solution at equilibrium, mg L^{-1}

k_1 — Rate constant of pseudo-first-order equation, min^{-1}

k_2 — Rate constant of pseudo-second-order equation, g mg^{-1} min^{-1}

k_3 — Rate constant of intraparticle diffusion equation, mg g^{-1} $min^{-0.5}$

m	—	Mass of adsorbent, g
T	—	Reaction temperature, K
q_e	—	Adsorption capacity at equilibrium, mg g^{-1}
$q_{e,1}$	—	Equilibrium adsorption capacity of pseudo-first-order equation, mg g^{-1}
$q_{e,2}$	—	Equilibrium adsorption capacity of pseudo-second-order equation, mg g^{-1}
a	—	Parameter of the Elovich equation, mg g^{-1}
b	—	Parameter of the Elovich equation, mg g^{-1} min^{-1}
q_t	—	Adsorption capacity at time t, mg g^{-1}
r^2	—	Correlation coefficient
SD	—	Standard deviation
s	—	Constant of intraparticle diffusion equation, mg g^{-1}
t	—	Contact time, min
V	—	Volume of adsorption solution, L

Acknowledgements

The authors would like to acknowledge four anonymous reviewers whose comments and advice greatly improved the quality of this article. This work was financially supported by the National Natural Science Foundation of China (NO.51273172) and Postgraduate Innovation Program of Jiangsu Province (SJCX190886).

References

[1] C.W. Abney, R.T. Mayes, T. Saito, S. Dai, Materials for the recovery of uranium from seawater, Chem. Rev., 117 (2017) 13935–14013.
[2] B. Aguila, Q. Sun, H. Cassady, C.W. Abney, B. Li, S. Ma, Design strategies to enhance amidoxime chelators for uranium recovery, ACS Appl. Mater. Interfaces, 11 (2019) 30919–30926.
[3] X.M. Wu, Q.X. Huang, Y. Mao, X.X. Wang, Y.Y. Wang, Q.H. Hu, H.Q. Wang, X.K. Wang, Sensors for determination of uranium: a review, TrAC, Trends Anal. Chem., 118 (2019) 89–111.
[4] D. Wang, J.N. Song, S. Lin, J. Wen, C.X. Ma, Y.H. Yuan, M. Lei, X.L. Wang, N. Wang, H. Wu, A marine-inspired hybrid sponge for highly efficient uranium extraction from seawater, Adv. Funct. Mater., 29 (2019) 1901009, doi: 10.1002/adfm.201901009.
[5] C. Tsouris, Uranium extraction: fuel from seawater, Nat. Energy, 4 (2017) 17022, doi: 10.1038/nenergy.2017.22.
[6] B.F. Parker, Z. Zhang, L. Rao, J. Arnold, An overview and recent progress in the chemistry of uranium extraction from seawater, Dalton Trans., 47 (2018) 639–644.
[7] D.R. Lovley, E.J.P. Phillips, Y.A. Gorby, E.R. Landa, Microbial reduction of uranium, Nature, 350 (1991) 413–416.
[8] E. Stalder, A. Blanc, M. Haldimann, V. Dudler, Occurrence of uranium in Swiss drinking water, Chemosphere, 86 (2012) 672–679.
[9] Y. Wang, L. Yu, R.T. Wang, Y. Wang, X.D. Zhang, A novel cellulose hydrogel coating with nanoscale Fe^0 for Cr(VI) adsorption and reduction, Sci. Total Environ., 726 (2020) 138625, doi: 10.1016/j.scitotenv.2020.138625.
[10] J.F. Chen, X.D. Zhang, X.Y. Shi, F.K. Bi, Y. Yang, Y.X. Wang, Synergistic effects of octahedral TiO_2-MIL-101(Cr) with two heterojunctions for enhancing visible-light photocatalytic degradation of liquid tetracycline and gaseous toluene, J. Colloid Interface Sci., 579 (2020) 37–49.
[11] Y. Wang, Y. Wang, L. Yu, R.T. Wang, X.D. Zhang, Highly effective microwave-induced catalytic degradation of Bisphenol A in aqueous solution using double-perovskite intercalated montmorillonite nanocomposite, Chem. Eng. J., 390 (2020) 124550, doi: 10.1016/j.cej.2020.124550.
[12] J.L. Wang, H. Chen, Catalytic ozonation for water and wastewater treatment: recent advances and perspective, Sci. Total Environ., 704 (2020) 135249, doi: 10.1016/j.scitotenv.2019.135249.
[13] X.D. Zhang, J.F. Chen, S.T. Jiang, X.L. Zhang, F.K. Bi, Y. Yang, Y.X. Wang, Z. Wang, Enhanced photocatalytic degradation of gaseous toluene and liquidus tetracycline by anatase/rutile titanium dioxide with heterophase junction derived from materials of Institut Lavoisier-125(Ti): degradation pathway and mechanism studies, J. Colloid Interface Sci., 588 (2021) 122–137.
[14] Y. Wang, R.T. Wang, L. Yu, Y. Wang, C.H. Zhang, X.D. Zhang, Efficient reactivity of $LaCu_{0.5}Co_{0.5}O_3$ perovskite intercalated montmorillonite and g-C_3N_4 nanocomposites in microwave-induced H_2O_2 catalytic degradation of bisphenol A, Chem. Eng. J., 401 (2009) 126057, doi: 10.1016/j.cej.2020.126057.
[15] Y.Q. Yang, Z.H. Zheng, W.Q. Ji, J.C. Xu, X.D. Zhang, Insights to perfluorooctanoic acid adsorption micro-mechanism over Fe-based metal organic frameworks: combining computational calculation with response surface methodology, J. Hazard. Mater., 395 (2020) 122686, doi: 10.1016/j.jhazmat.2020.122686.
[16] X.X. Wang, X. Li, J.Q. Wang, H.T. Zhu, Recent advances in carbon nitride-based nanomaterials for the removal of heavy metal ions from aqueous solution, J. Inorg. Mater., 35 (2020) 260–270.
[17] X. Zhong, W. Liang, Z.P. Lu, B.W. Hu, Highly efficient enrichment mechanism of U(VI) and Eu(III) by covalent organic frameworks with intramolecular hydrogen-bonding from solutions, Appl. Surf. Sci., 504 (2020) 144403, doi: 10.1016/j.apsusc.2019.144403.
[18] N.S. Alharbi, B.W. Hu, T. Hayat, S.O. Rabah, A. Alsaedi, L. Zhuang, X.K. Wang, Efficient elimination of environmental pollutants through sorption-reduction and photocatalytic degradation using nanomaterials, Front. Chem. Sci. Eng., 14 (2020) 1124–1135.
[19] L.C. Tan, Y.L. Wang, Q. Liu, J. Wang, X.Y. Jing, L.H. Liu, J.Y. Liu, D.L. Song, Enhanced adsorption of uranium(VI) using a three-dimensional layered double hydroxide/graphene hybrid material, Chem. Eng. J., 259 (2015) 752–760.
[20] S.Y. Huang, H.W. Pang, L. Li, S.B. Jiang, T. Wen, L. Zhuang, B.W. Hu, X.K. Wang, Unexpected ultrafast and high adsorption of U(VI) and Eu(III) from solution using porous Al_2O_3 microspheres derived from MIL-53, Chem. Eng. J., 353 (2018) 157–166.
[21] L. Xie, J.Y. Wang, D.W. Yuan, C. Shi, X. Cui, H. Zhang, Q. Liu, Q.X. Liu, H.B. Zeng, Interaction mechanisms between air bubble and molybdenite surface: impact of solution salinity and polymer adsorption, Langmuir, 33 (2017) 2353–2361.
[22] M. Sprynskyy, T. Kowalkowski, H. Tutu, E.M. Cukrowska, B. Buszewski, Adsorption performance of talc for uranium removal from aqueous solution, Chem. Eng. J., 171 (2011) 1185–1193.
[23] T.N. Zhang, X.W. Xu, L. Dong, Z.Y. Tan, C.L. Liu, Molecular dynamics simulations of uranyl species adsorption and diffusion behavior on pyrophyllite at different temperatures, Acta. Phys.-Chim. Sin., 33 (2017) 2013–2021.
[24] M.H. Khan, P. Warwick, N. Evans, Spectrophotometric determination of uranium with arsenazo-III in perchloric acid, Chemosphere, 63 (2006) 1165–1169.
[25] H. Veisi, S.A. Mirshokraie, H. Ahmadian, Synthesis of biaryls using palladium nanoparticles immobilized on metformine-functionalized polystyrene resin as a reusable and efficient nanocatalyst, Int. J. Biol. Macromol., 108 (2018) 419–425.
[26] S. Bhavsar, G.B. Patel, N.L. Singh, Investigation of optical properties of aluminium oxide doped polystyrene polymer nanocomposite films, Physica B, 533 (2018) 12–16.
[27] X.Y. Shi, X.D. Zhang, F.K. Bi, Z.H. Zheng, L.J. Sheng, J.C. Xu, Z. Wang, Y.Q. Yang, Effective toluene adsorption over defective UiO-66-NH_2: an experimental and computational exploration, J. Mol. Liq., 316 (2020) 113812, doi: 10.1016/j.molliq.2020.113812.
[28] S.H. Ri, F.K. Bi, A. Guan, X.D. Zhang, Manganese-cerium composite oxide pyrolyzed from metal organic framework supporting palladium nanoparticles for efficient toluene oxidation, J. Colloid Interface Sci., 586 (2021) 836–846.
[29] J.P. Zhou, W.Q. Cai, Z.C. Yang, Q. Xia, J.W. Chen, J.J. Fan, C.H. Du, *N,N*-dimethylformamide assisted facile hydrothermal synthesis of boehmite microspheres for highly effective removal

of Congo red from water, J. Colloid Interface Sci., 583 (2021) 128–138.
[30] K. Ohsawa, M. Murata, H. Ohshima, Zeta potential and surface charge density of polystyrene-latex; comparison with synaptic vesicle and brush border membrane vesicle, Colloid Polym. Sci., 264 (1986) 1005–1009.
[31] Z. Wang, Y. Xie, Z. Lei, Y.X. Lu, G.Y. Wei, S. Liu, C. Xu, Z.C. Zhang, X.K. Wang, L.F. Rao, J. Chen, Quantitative analysis of surface sites on carbon dots and their interaction with metal ions by a potentiometric titration method, Anal. Chem., 91 (2019) 9690–9697.
[32] S. Black, J.R. Ferrell III, Determination of carbonyl groups in pyrolysis bio-oils using potentiometric titration: review and comparison of methods, Energy Fuels, 30 (2016) 1071–1077.
[33] F.X. Zhang, M. Lang, J.W. Wang, W.X. Li, K. Sun, V. Prakapenka, R.C. Ewing, High-pressure U_3O_8 with the fluorite-type structure, J. Solid State Chem., 213 (2014) 110–115.
[34] S.B. Donald, M.L. Davisson, A.J. Nelson, XPS Investigation on changes in UO_2 speciation following exposure to humidity, MRS Adv., 1 (2016) 2993–2997.
[35] G.C. Allen, N.R. Holmes, Surface characterisation of α-, β-, γ-, and δ-UO_3 using X-ray photoelectron spectroscopy, J. Chem. Soc. Dalton Trans., 12 (1987) 3009–3015.
[36] A. Schierz, H. Zänker, Aqueous suspensions of carbon nanotubes: surface oxidation, colloidal stability and uranium sorption, Environ. Pollut., 157 (2009) 1088–1094.
[37] G.H. Wang, J.S. Liu, X.G. Wang, Z.Y. Xie, N.S. Deng, Adsorption of uranium(VI) from aqueous solution onto cross-linked chitosan, J. Hazard. Mater., 168 (2009) 1053–1058.
[38] Y.S. Ho, G. McKay, The kinetics of sorption of divalent metal ions onto sphagnum moss peat, Water Res., 34 (2000) 735–742.
[39] Y. Liu, Y.Z. Huo, X.X. Wang, S.J. Yu, Y.J. Ai, Z.S. Chen, P. Zhang, L. Chen, G. Song, N.S. Alharbi, S.O. Rabah, X.K. Wang, Impact of metal ions and organic ligands on uranium removal properties by zeolitic imidazolate framework materials, J. Cleaner Prod., 278 (2021) 123216, doi: 10.1016/j.jclepro.2020.123216.
[40] X. Lu, D.X. Zhang, A.T. Reda, C. Liu, Z. Yang, S.S. Guo, S.T. Xiao, Y.G. Ouyang, Synthesis of amidoxime-grafted activated carbon fibers for efficient recovery of uranium(VI) from aqueous solution, Ind. Eng. Chem. Res., 41 (2017) 11936–11947.
[41] H. Pang, H. Tang, J. Wang, X. Wang, S. Yu, Ternary layered double hydroxide supported sulfide NZVI: efficient U(VI) elimination and mechanism, J. Inorg. Mater., 32 (2020) 381–389.
[42] A.C.M. Lamb, F. Grieser, T.W. Healy, The adsorption of Uranium(VI) onto colloidal TiO_2, SiO_2 and carbon black, Colloids Surf., A, 499 (2016) 156–162.
[43] Y.G. Zhao, J.X. Li, L.P. Zhao, S.W. Zhang, Y.S. Huang, X.L. Wu, X.K. Wang, Synthesis of amidoxime-functionalized Fe_3O_4@SiO_2 core–shell magnetic microspheres for highly efficient sorption of U(VI), Chem. Eng. J., 235 (2014) 275–283.
[44] H. Wang, L.J. Ma, K.C. Cao, J.X. Geng, J. Liu, Q. Song, X.D. Yang, S.J. Li, Selective solid-phase extraction of uranium by salicylideneimine-functionalized hydrothermal carbon, J. Hazard. Mater., 229–230 (2012) 321–330.
[45] Y. Liu, L.Y. Yuan, Y. Yuan, J.H. Lan, Z.J. Li, Y.X. Feng, Y.L. Zhao, Z.F. Chai, W.Q. Shi, A high efficient sorption of U(VI) from aqueous solution using amino-functionalized SBA-15, J. Radioanal. Nucl. Chem., 292 (2012) 803–810.
[46] Y.S. Ho, J.C.Y. Ng, G. Mckay, Kinetics of pollutant sorption by biosorbents: review, Sep. Purif. Methods, 29 (2000) 189–232.
[47] M.M. Abdallah, M.N. Ahmad, G. Walker, J.J. Leahy, W. Kwapinski, Batch and continuous systems for Zn, Cu, and Pb metal ions adsorption on spent mushroom compost biochar, Ind. Eng. Chem. Res., 58 (2019) 7296–7307.
[48] W. Liu, L. Zhang, F. Chen, H. Wang, Q. Wang, K. Liang, Efficiency and mechanism of adsorption of low-concentration uranium from water by a new chitosan/aluminum sludge composite aerogel, Dalton Trans., 49 (2020) 3209–3221.
[49] A.H. Sulaymon, W.M. Abood, Equilibrium and kinetic study of the adsorption of reactive blue, red and yellow dyes onto activated carbon and barley husk, Desal. Water Treat., 52 (2014) 5485–5493.
[50] P. Li, P. Chen, Z.P. Liu, S.Y. Nie, X.G. Wang, G.H. Wang, W.M. Zhang, H. Chen, L.Z. Wang, Highly efficient elimination of uranium from wastewater with facilely synthesized Mg-Fe layered double hydroxides: optimum preparation conditions and adsorption kinetics, Ann. Nucl. Energy, 140 (2020) 107140, doi: 10.1016/j.anucene.2019.107140.
[51] Z.Q. Wen, K.H. Huang, Y.Q. Niu, Y.X. Yao, S. Wang, Z.F. Cao, H. Zhong, Kinetic study of ultrasonic-assisted uranium adsorption by anion exchange resin, Colloids Surf., A., 585 (2020) 124021, doi: 10.1016/j.colsurfa.2019.124021.
[52] S.T. Zhuang, J.L. Wang, Poly amidoxime functionalized carbon nanotube as an efficient adsorbent for removal of uranium from aqueous solution, J. Mol. Liq., 319 (2020) 114288, doi: 10.1016/j.molliq.2020.114288.
[53] H.J. Liu, S.B. Xie, J. Liao, T.R. Yan, Y.J. Liu, X.H. Tang, Novel graphene oxide/bentonite composite for uranium(VI) adsorption from aqueous solution, J. Radioanal. Nucl. Chem., 317 (2018) 1349–1360.